A&A 545, A145 (2012)
DOI: 10.1051/0004-6361/201118665

Astronomy & Astrophysics

Herschel far-IR observations of the Chamaeleon molecular cloud complex⋆

Chamaeleon I: A first view of young stellar objects in the cloud

E. Winston[1], N. L. J. Cox[2], T. Prusti[1], B. Merín[3], A. Ribas[3], P. Royer[2], R. Vavrek[3], E. Puga[3], Ph. André[4], A. Men'shchikov[4], V. Könyves[4], Á. Kóspál[1], C. Alves de Oliveira[3], G. L. Pilbratt[1], and C. Waelkens[2]

[1] ESTEC (SRE-SA), European Space Agency, Keplerlaan 1, 2201 AZ Noordwijk ZH, The Netherlands
e-mail: ewinston@rssd.esa.int
[2] Instituut voor Sterrenkunde, KU Leuven, Celestijnenlaan 200D, 3001 Leuven, Belgium
[3] *Herschel* Science Centre, European Space Astronomy Centre (ESA), PO Box 78, 28691 Villanueva de la Cañada, Madrid, Spain
[4] Laboratoire AIM Paris–Saclay, CEA/DSM–CNRS–Université Paris Diderot, IRFU, Service d'Astrophysique, Centre d'Études de Saclay, Orme des Merisiers, 91191 Gif-sur-Yvette, France

Received 12 December 2011 / Accepted 17 July 2012

ABSTRACT

Context. The *Herschel* Gould Belt survey of nearby star forming regions is providing great insights into the early stages of the formation and the evolution of stars and their circumstellar disks. The Chamaeleon I dark cloud is an elongated region of dense dust and gas where star formation is ongoing in two centres, a northern region centred on Ced 112 and a southern cluster subdivided into the two regions Ced 110 and 111.

Aims. In this initial study we present *Herschel* data of previously identified young stellar objects (YSOs) in the cluster, focusing on the spatial distribution of the YSOs and the determination of the relative colours of the protostars and the disk-bearing stars in Chamaeleon I.

Methods. Chamaeleon I has been observed as part of the *Herschel* Gould Belt Survey, using the PACS and SPIRE parallel mode imaging at 70, 160, 250, 350, and 500 μm. Source extraction was performed using the *getsources* software.

Results. We have detected 397 sources over the five available PACS and SPIRE bands, and through comparison with previously identified objects in the cluster we have identified 49 YSOs, 4 bright nebular emission features, five CO clumps, and twenty-eight candidate prestellar or starless cores in the *Herschel* sample. The remaining sample consists of candidate prestellar cores, condensations within the cloud, or background galaxies. The *Herschel* detected YSOs are highly clustered and mainly associated with the three known Cederblad groups. The observations clearly show that the young stars are forming coincident with the denser regions of cold dust and gas, visible at longer *Herschel* wavelengths. Those YSOs detected with *Herschel* were found to have an IRAC $m_{3.6\ \mu\mathrm{m}} < 10$. No difference was found in the *Herschel* colours between the class I and class II young stars, however the class I sources were brighter than the class II at most *Herschel* wavelengths. One class III star and three transition disks are detected.

Key words. circumstellar matter – stars: pre-main sequence – stars: protostars – infrared: stars

1. Introduction

Star formation occurs in the hearts of cold molecular clouds, where young stars begin their lives shrouded in the envelopes of cold dust and gas from which they condense. As the protostar evolves infalling material forms a circumstellar disc from which planetary systems may later form. During these earliest stages, most of the emission from these protostars is in the form of reprocessed stellar radiation emitted at longer, far-infrared (far-IR) wavelengths. These very earliest stages of star formation have remained hidden from us until the advent of modern infrared charge-coupled devices and bolometric arrays. The *Herschel* Space Observatory (Pilbratt et al. 2010) provides an unprecedented view of the earliest stages of star formation. The PACS (Poglitsch et al. 2010) and SPIRE (Griffin et al. 2010) instruments provide the capability for large scale mapping of star forming regions in the far-IR in relatively short amounts of time. One of the goals of the *Herschel* Gould Belt survey (André et al. 2010) is to obtain a census of prestellar cores and protostars in nearby clouds.

Chamaeleon I (hereafter Cha I) is a nearby region of low mass star formation, located at a distance of 160–180 pc (Whittet et al. 1997, and references therein), in a complex which also contains Chamaeleon II & III and Musca (Luhman 2008). The entire Cha I cloud covers an area of ~5 deg^2 and, at this distance, is one of the closest regions of star formation to the Earth. From spectroscopic surveys of confirmed young stellar objects (YSOs), the age of the cluster has been found to be ~2 Myr (Luhman 2008, and references therein). Previously, the region has been observed from the optical to the radio by *Spitzer*, SEST, ISOCAM, 2MASS, and DENIS, among others (Luhman et al. 2008; Haikala et al. 2005; Persi et al. 2000; Gomez & Kenyon 2001; Cambresy et al. 1998). Extinction maps towards the cloud give values of A_V in the range 5–20 mag, implying that even the protostars are not too deeply embedded, giving us an unimpeded view of the entire population of the region. The cloud is

⋆ *Herschel* is an ESA space observatory with science instruments provided by European-led Principal Investigator consortia and with important participation from NASA.

separated into two main parts: the northern cluster centred on the Herbig star HD 97300 and the reflection nebula Ced 112 (Cederblad 1946), and the southern clusters including two reflection nebulae Ced 110 and Ced 111 and the Infrared Nebula (Schwartz & Henize 1983, IRN). In his article in the *Handbook of Star Forming Regions* Luhman (2008) provides an in-depth and detailed review of the entire Chamaeleon complex and the population of YSOs within.

In this initial paper on the Chamaeleon complex, we present the first results of *Herschel* Gould Belt survey of Cha I, detailing the data reduction, map making process, and source extraction. We then present a comparison of the *Herschel* detected objects with those in previous catalogues, primarily focusing on the recent *Spitzer* surveys of the cloud (Luhman et al. 2008; Kim et al. 2009; Manoj et al. 2011), which provide reliable evolutionary classifications for the known members. Finally we discuss the mid- and far-IR properties of the young stars detected with *Herschel* by evolutionary class.

2. Observations and data reduction

The Cha I region was observed by *Herschel* as part of the Gould Belt survey (André et al. 2010). The observations (OBSIDS 1342213178, 1342213179) were performed using the parallel mode covering an area of ~5.4 deg^2 for both PACS (at 70 and 160 μm) and SPIRE (at 250, 350 and 500 μm) instruments, with a scanning speed of 60″ s^{-1}. The field was observed twice by performing cross-linked scans in two nearly orthogonal scan directions. The total observing time was ~8 h, each observation being ~4 h. The observing date was the 22nd of January 2011 for both observing directions. The full width at half maximum of the point-spread-functions (PSFs) for PACS in the parallel mode at 70 and 160 μm are 5.8″ × 12″ and 11.6″ × 15.4″, respectively. Beam sizes are 18.1″, 25.2″, and 36.9″, for 250, 350, and 500 μm, respectively for SPIRE.

The data were reduced using the *Herschel* Interactive Processing Environment (HIPE, Ott 2010) version 7 using both the photProject and *madMap* algorithms for PACS observations, and *naiveMap* algorithm for SPIRE. However, the pipelines contained in this version produced some problems due to the characteristics of this kind of star forming regions: the baseline-removal part of the mapping algorithm produced negative flux values (overshooting) in some regions located next to the bright filamentary structures in the scan directions. For this reason we decided to use *scanamorphos* (Roussel et al. 2012) version 12, a map-making software designed to take advantage of the redundancy of the observations. This procedure allowed us to get rid of the negative flux values and the corresponding artifacts in the maps, making the overall photometric measurements more reliable when compared to the output from the HIPE maps (both for the PACS and SPIRE instruments). Scanamorphos maps suffer much less from areas of overshooting, in fact these features were no longer present. Checking for consistency between the photometry from HIPE and Scanamorphos maps for clearly detected sources unaffected by artifacts (>100 mJy) in both maps, we find no relevant differences in the photometry.

2.1. Source extraction

Source extraction was performed using *getsources* (Men'shchikov et al. 2010, 2012), which is designed specifically for use with *Herschel* data. The mosaics are prepared using *prepareobs*, part of the *getsources* package, which resamples the mosaics to a 3″ pixel scale. Unlike other source extraction algorithms, the new method analyzes fine spatial decompositions of original images across a wide range of scales and across all wavelengths. As part of its multi-wavelength design, *getsources* removes the noise and background fluctuations from the decomposed images separately in each band, and constructs a set of wavelength-independent detection images that preserve information in both spatial and wavelength dimensions as well as possible. Sources are detected in the combined detection images by following the evolution of their segmentation masks across all spatial scales. Measurements of the source properties are performed in the original images at each wavelength after the background has been subtracted by interpolation under the sources' "footprints" and after overlapping sources have been deblended. Based on the results of the initial extraction, detection images are "flattened" to produce much more uniform noise and background fluctuations in preparation for the second, final extraction. A more detailed description of the *getsources* software is provided in the forthcoming paper by Men'shchikov et al. (2012).

The final merged source catalogue provided 397 detections at the five available bandpasses of PACS and SPIRE over the whole Cha I field of the initial *getsources* extraction run with a combined significance across all detected bandpasses >7σ, where 347 have detections in more than one band. No constraints were placed a priori on the source detection, such as for source size, minimum flux level, or detection at multiple wavelengths, to ensure that no known source was missed. The fluxes returned by *getsources* include the peak flux of each detection and the total flux within an ellipse determining its extent on the sky at each specific wavelength. In this study, we use the measure of the total flux for each object detected. Of the 306 sources with detections at 250 μm, 49 have major axis >30″, greater than 1.65 × FWHM(PSF) at 250 μm. The uncertainties were also derived by the *getsources* routine. Typical uncertainties on the fluxes at each wavelength are less than 20%, with ~75% having uncertainties less than 40% of the total measured flux. For this paper the lower limit for reporting fluxes was set at ~0.1 Jy for each of the PACS 70, 160 μm, and SPIRE 250, 350, 500 μm bands. Twenty-six of the sources were detected in all five available bands, with forty-one detected at all four bands from 160 to 500 μm, and two hundred only detected in some bands longward of 160 μm. The remaining 130 sources are detected only in bands shortward of 250 μm.

3. Results

3.1. Cross correlation with other catalogues

The Cha I region, given its close proximity to us, has been extensively studied at other wavelengths over the decades. To date, more than 200 young stars have been identified as members of the Cha I cloud. Previous studies using X-ray, optical, near-IR, mid-IR, and sub-mm instruments have provided a comprehensive view of young members from the young protostars (class I) to the evolved diskless members (class III). *Herschel* provides some of the highest resolution observations to date in the far-IR to submm; from these data we can identify the protostars (class 0 and class I), prestellar cores, and the emission from the remnant envelopes and cold outer disks of the more evolved class II young stars. Figure 1 shows the three-band false-colour image of a *Herschel* PACS and SPIRE view of Cha I, where the PACS 160 μm band is shown in blue, SPIRE 250 μm in green, and SPIRE 500 μm in red. The three Cederblad regions are marked on the image. While some of the emission at the

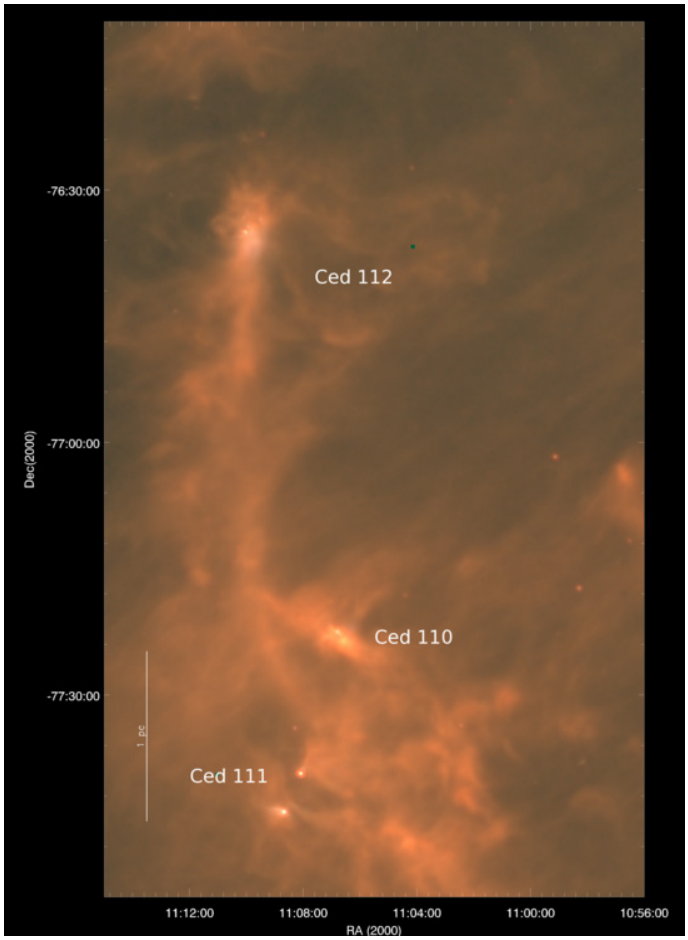

Fig. 1. Three-band false-colour image of the Chamaeleon I region, with PACS 160 μm in blue, SPIRE 250 μm in green and SPIRE 500 μm in red. The northern region, centred on Ced 112 and HD 97300, and two southern clusters, Ced 110 and Ced111 are visible. North is up and east is to the left.

shorter wavelengths arises from stellar sources, the cold dust emits strongly at 500 μm, where the underlying structure of the cloud is clearly observed.

To correctly identify the *Herschel* sources we mapped the detections and matched sources to those at shorter wavelengths where the positional offsets were less than 5″. Given the lower positional accuracy in the *Herschel* astrometry due to the larger beam size of *Herschel* when compared to those at shorter wavelengths, we did not rely on blind matching only, but visually checked each object against the positions of objects in the *Spitzer*, ISOCAM, DENIS, and 2MASS catalogues and utilised the online *Aladin* software to compare the *Herschel* sources to the DSS optical images and the SIMBAD catalogue.

Luhman (2008) presents a review of previous surveys of the region, where they confirm a total of 237 YSOs associated with Cha I. Luhman et al. (2008) present a *Spitzer* IRAC and MIPS survey of Cha I where they report the detection of 204 YSOs in the mid-IR. These YSOs were classified using the slope of their spectral energy distributions (SEDs) and their positions on various colour–colour diagrams. Of these 204 YSOs, they found five class I (two in the northern, three in the southern groupings), ten flat spectrum (two in the north, eight in the south), ninety-four class II (43 north, 51 south), and ninety-five class III (44 north, 51 south). Of the 397 *Herschel* sources, a total of forty-nine, are matched to YSOs identified in the Luhman (2008) catalogue. Of these 49, four are class I (one in the north, three in the south) and one, Cha MMS1 is very young class 0 object (Reipurth et al. 1996), six are flat spectrum (one in the north, five in the south), thirty-four are in evolutionary class II, and three are considered to be transition disc objects: CS Cha, SZ Cha, and T54. The remaining source is Ced 110 IRS2, a class III, diskless member of Cha I, which was also identified in the *Herschel* data, indicating that it retains circumstellar material in an outer disk.

Recently, Belloche et al. (2011) presented a LABOCA 870 μm map of the Cha I cloud, and reported the detection of 59 starless cores and 21 sources associated with YSOs. When compared to the *Herschel* detections, we find 51 sources in common between the two catalogues, with an additional fourteen possible matches where the offset is greater than 25″. Of the fifty-one common detections, all 21 of the Belloche detections associated with known YSOs are also detected with *Herschel*, two are associated with the ring of nebular emission surrounding HD 97300 (Kóspál et al. 2012) and the remaining twenty-eight are associated with candidate prestellar cores which lack near or mid-IR detections. We likely do not find counterparts for the other twenty-nine 870 μm detections due to different source extraction algorithms, the difference in the resolution between the catalogues, and the requirements for greater than 7-σ detections in the *Herschel* catalogue.

Haikala et al. (2005) used the SEST telescope to observe the Cha I region in $C^{18}O$, ^{13}CO, and $C^{17}O$. They identified 71 clumps, to which we find 9 counterparts in the *Herschel* dataset with positional accuracy <25″. Four of these appear to correspond to Belloche et al. (2011) sources, adding five new candidates to the list of *Herschel* sources.

The region has been observed in X-rays with ROSAT by Lawson et al. (1996), with *Chandra* by Feigelson & Lawson (2004) and with XMM by Stelzer et al. (2004) to look for high energy emission from young stars with the purpose of studying their X-ray properties and to identify any class III diskless members of the cluster, which do not exhibit excess emission in the IR, but are bright in X-rays (Guenther et al. 2007) with emission 10^3–10^4 times their main sequence counterparts. Combining all three surveys, twenty-one of the 49 *Herschel* and *Spitzer* detected YSOs have counterparts in the X-ray catalogues.

Persi et al. (2000) presented a mid-IR study of Cha I cloud using ISOCAM on the Infrared Space Observatory (ISO). In the paper they reported the detection of 108 young stars, mainly class II, in two broad band filters at 6.7 μm and 14.3 μm covering a 0.5 square degree field of the cloud. Of the 108 young members detected with ISOCAM, 28 have counterparts detected in the *Herschel* field.

A survey of 82 young stars and brown dwarfs in Cha I was carried out by Manoj et al. (2011) using the *Spitzer* Infrared Spectrograph (IRS) mid-IR spectrograph. Their Table 3 shows that of the 49 known YSOs in our *Herschel* sample, sixteen are known to be in multiple systems. They also updated the evolutionary classification of the previously known YSOs and found that many of the disks show evidence of dust settling and evolution in the mid-IR. Kim et al. (2009) presented a *Spitzer* IRS survey of a number of transition disc candidates in Cha I, concluding SZ Cha, CS Cha, and T54 to be transition disks.

3.2. Herschel catalogue of known objects

The final *getsources* catalogue for the region included 397 sources with detections in one or more of the five available *Herschel* bandpasses. Having compared the *Herschel* catalogue

to those at all other available wavelengths, we match 86 of the 397 *Herschel* detections to known sources. This includes 49 YSOs, two outflow features, two emission features near HD 97300, discussed in detail in Kóspál et al. (2012), 28 candidate prestellar/starless cores (Belloche et al. 2011), and five CO clumps (Haikala et al. 2005). Table 1 presents the identifications, evolutionary classification, the *Herschel* fluxes, and the spectral types for the identified YSOs in Cha I. The remaining 311 objects were not previously identified as young stars, emission features or cores in the cluster. The source extractions are preliminary at this point, hence the details of those sources not identified as a previously known YSO are not given here, but will be presented in a later publication, pending a more complete analysis of their SEDs. These may be deeply embedded protostars, prestellar cores, or condensations of dust in the filamentary structure of the cloud. These detections may also be background extragalactic contaminants. It is likely that the majority of the point-like sources that are located off-cloud in regions of lower A_V are galaxies. Clements et al. (2010) estimate the number counts of galaxies in the *Herschel* SPIRE 250 μm field as 10–20 per sq. deg. at 100 mJy, rising to ~100 galaxies per sq. deg. at 50 mJy; given the ~5.4 sq. deg. coverage of the Cha I cloud and our sensitivity limits at ~100 mJy, we could therefore expect a few hundred galaxies in the field. This number may be further reduced by the interstellar extinction over much of the observed field. In this paper, only the photometry of the previously known sources will be included in the discussion of the *Herschel* photometry, where a general comparison will be made between the known young stars and candidate cores.

While the northern region, Ced 112, contains a smaller population than the southern one, Ced 110 and 111, the two regions possess similar properties statistically, and this holds true with the inclusion of the *Herschel* data. Comparing to the Luhman et al. (2008) catalogue, we detect all but one of the known class I protostars with *Herschel*. The nondetected class I is seen only faintly, and it was not reliably separated from the cloud emission. The detection fraction with evolutionary class falls off rapidly; with 1 of 2 flat spectrum sources in the north, and 5 of 8 (63%) in the southern region detected. For the class II sources, which are distributed more evenly throughout the region, the overall detection fraction drops to 34%. We detect only one of the known class III sources over the whole cloud and only three transition disks. There is no difference in the fractions of previously known sources seen with *Herschel* in the northern Ced 112 region compared to the southern, Ced 110 and 111, region.

4. Discussion

4.1. *Spitzer* colours of Herschel detected YSOs

Figure 2a shows the traditional *Spitzer* IRAC colour–colour figure (ccd) of the known YSOs in Chamaeleon I, while Fig. 2b shows the *Spitzer* IRAC-MIPS ccd of those YSOs. The grey dots are the members listed in Luhman et al. (2008), the black squares are those YSOs also detected with *Herschel*. The fluxes are plotted without dereddening of the IRAC data. There is little discernible difference in colour between those young stars detected by *Herschel* and those that are not, with no obvious trend towards redder IRAC colours discernible. This would imply that the extent and/or structure of the inner ~1–5 AU disk, detected in the mid-IR with IRAC, does not have a strong bearing on whether or not an outer disc (10 to >100 AU) or remnant envelope will be detected at the longer *Herschel* wavelengths. Only one source is detected in the class III/transition disc region, the transition disc CS Cha. Similarly, only one of the class III sources is detected by *Herschel*.

Figure 3 shows the [3.6] vs. [3.6−4.5] colour–magnitude figure (cmd) of the *Spitzer* YSOs with the *Herschel* sources as above. Here it can clearly be seen that it is the brighter objects that have been detected with *Herschel*. From a total number of 150 YSOs on this cmd, 20/25 or 80% are detected with *Herschel* for $m_{3.6} < 8.5$, 26/61 or 43% are detected with *Herschel* for $m_{3.6} < 10$, and 4/89 or 4% are detected for $m_{3.6} > 10$. The *Herschel* detections are complete for objects with [3.6−4.5] colour >0.6 and $m_{3.6} < 10$.

In order to investigate further, the values of α_{2-8}, the slope of the SED calculated between the K_S band and the IRAC 8μm wavelength, of both the *Herschel* detected class II and the class II members not detected by *Herschel* were examined. The value of α_{2-8} is interpreted as a measure of the amount of infrared excess emission a star possesses; positive values indicating a protostar with emission from an envelope and negative values >–2 indicating a class II young star. The α_{2-8} values utilised here were those presented in Table 8 of Luhman et al. (2008). The median α_{2-8} value of the class II sources detected with *Herschel* is -1.21 ± 0.77. The median α_{2-8} of the class II sources not detected with *Herschel* is -1.44 ± 0.55. The uncertainties presented are the standard deviation of the α_{2-8} values. These results are statistically similar; there is no suggestion that the sources with stronger emission from their inner disks are more likely to be detected than those with weaker emission.

4.2. Clustering of Herschel detected YSOs

Figure 4 shows the contours of the 500 μm SPIRE mosaic in grey, which traces the densities of cold dust in the cloud. Overlaid on the contours are the positions of the Luhman et al. (2008) YSOs detected in the *Spitzer* IRAC and MIPS observations, shown by the open circles. The filled circles are those of the YSOs that are also detected at *Herschel* wavelengths. The "*x*" symbols mark the locations of the twenty-nine *Herschel* detections with a counterpart in the Belloche et al. (2011) LABOCA catalogue. These objects include candidate class 0 protostars and prestellar or starless cores; they are located either in one of the three main Cederblad groups or are adjacent to other *Spitzer* identified YSOs. Further modelling of the SEDs of these sources will provide a better understanding of their nature, and will be presented in a later paper. The majority of the previously identified YSOs that are detected with *Herschel* are found to be clustered in the core of the northern region surrounding HD97300/Ced 112, and in the two clusters Ced 110 and Ced 111 to the south. The YSOs detected with *Herschel* are more likely to be contiguous with the denser regions of cold dust traced by the 500 μm emission than those that are not. The percentage of *Herschel* detected YSOs within the 50% contour in Fig. 4 is 60% (29/49), the percentage of YSOs not detected with *Herschel* within the 50% contour is 28% (52/183). In this regard, Cha I is similar to other clusters, such as Aquila (André et al. 2010) and IC 5146 (Arzoumanian et al. 2011) where the sources have been found to be contiguous with the filaments in the clouds; future work on the filamentary structure of the Chamaeleon clouds will indicate whether the young stars also trace the filamentary structure of Cha I (Alves de Oliveira et al., in prep.).

The YSOs detected with *Herschel* are also the brightest YSOs in the mid-IR as shown in Fig. 3. This may at first suggest that these are the more massive stars with correspondingly more massive outer disks and are therefore detected in *Herschel* due to their increased emission. However, from their spectral

Table 1. Identifiers and fluxes of *Herschel* detected YSOs in Cha I.

Coordinate identifier	Other identifier	Evol. class	70 μm Jy	160 μm Jy	250 μm Jy	350 μm Jy	500 μm Jy	Spectral type	References sp. type
2M J10563044-7711393	SY Cha, T4, Sz3, Bel17	II	0.4 ± 0.1	0.6 ± 0.1	0.6 ± 0.2	0.6 ± 0.1	0.4 ± 0.2	K2, M0, M0.5	5, 17, 19
2M J10581677-7717170	SZ Cha, Glass V, T6, Bel7	II/TD	3.1 ± 0.1	3.3 ± 0.1	2.1 ± 0.1	1.7 ± 0.1	1.0 ± 0.1	K0	2
2M J10590697-7701403	CR Cha, T8, Sz6, CHXR10	II	1.3 ± 0.1	2.4 ± 0.1	1.9 ± 0.1	1.6 ± 0.1	0.9 ± 0.1	G8, K0, K2, K2	5, 6, 2, 3
2M J11022491-7733357	CS Cha, T11, P1, Bel10	TD	2.6 ± 0.1	1.9 ± 0.1	1.2 ± 0.2	0.8 ± 0.2	0.5 ± 0.2	K2, K2, K5, M0, K6	5, 6, 2, 3, 1
2M J11040909-7627193	CT Cha, T14, CHXR13	II	0.6 ± 0.1	0.6 ± 0.1	0.5 ± 0.1	0.4 ± 0.1	0.2 ± 0.1	K7, K5	3, 1
2M J11042275-7718080	HH48, T14A, P4, Bel22	I	0.6 ± 0.1	0.7 ± 0.1	0.6 ± 0.1	0.5 ± 0.1	0.3 ± 0.1	K6-M0	1
2M J11044258-7741571	ISO52, B18, P5	II	0.1 ± 0.1	...	...	...	...	M4, M4.5	1, 14
2M J11061540-7721567	Ced110-IRS2, T21	III	2.9 ± 0.1	7.0 ± 1.9	...	...	...	G3-G7	13
2M J11062554-7633418	ESO Ha 559	II	0.2 ± 0.1	0.3 ± 0.1	0.2 ± 0.1	0.2 ± 0.1	...	M6, M5. 25	4, 1
2M J11063460-7723340	Cha MMS-1	0	0.2 ± 0.1	25.3 ± 1.5	50.3 ± 2.5	48.2 ± 2.2	25.1 ± 1.4	...	...
2M J11064658-7722325	Ced110-IRS4, P9, Bel5	I	8.0 ± 0.1	5.1 ± 0.3	2.9 ± 0.4	1.6 ± 0.5	...	...	...
2M J11070919-7723049	Ced110-IRS6, P11	Flat	3.5 ± 0.1	4.9 ± 0.6	2.5 ± 0.9	2.8 ± 0.9	2.9 ± 0.8	...	...
2M J11071206-7632232	UZ Cha, T24, CHXR75	II	0.2 ± 0.1	0.2 ± 0.1	0.1 ± 0.1	...	...	M0.5	1
2M J11071622-7723068	ISO97, C8	Flat	...	1.5 ± 0.6	1.3 ± 0.8	...	0.3 ± 0.8	M1	4
2M J11071915-7603048	T25, Cam1-47, Sz18	II	0.5 ± 0.1	0.4 ± 0.1	0.2 ± 0.1	0.2 ± 0.1	...	...	...
2M J11072074-7738073	DI Cha, T26, P14	II	2.1 ± 0.2	1.4 ± 0.4	...	...	...	G2, G2, G2, G2, G2	5, 6, 2, 3, 15
2M J11072142-7722117	B35, P15, Bel20	Flat	0.3 ± 0.1	0.3 ± 0.5	...	...	0.4 ± 0.7	M2	4
2M J11074366-7739411	FI Cha, HM15, P17, Bel28	II	0.4 ± 0.1	0.4 ± 0.3	0.4 ± 0.4	...	...	M0.5, M0.5, M1, M0	2, 17, 12, 7
2M J11075730-7717262	CHXR30b, P20	II	0.2 ± 0.1	...	...	...	...	M0.75-1.75	1
2M J11075792-7738449	FK Cha, HM16, P18, Bel13	Flat	8.0 ± 0.1	5.1 ± 0.3	2.9 ± 0.4	1.6 ± 0.5	...	K7, K4-K6	12, 7
2M J11080148-7742288	VW Cha, T31, P21	II	1.2 ± 0.6	0.5 ± 0.7	...	...	...	K2, K5-K7, M0.5, K8	3, 16, 21, 1
2M J11080297-7738425	ISO126, C11	II	4.0 ± 0.1	1.5 ± 0.3	1.2 ± 0.4	0.3 ± 0.5	...	M2, M1, 25	4, 1
2M J11080329-7739174	HD97048, T32, P22, Bel1	II	53.7 ± 0.3	53.8 ± 0.4	33.5 ± 0.4	21.5 ± 0.4	10.9 ± 0.4	B9.5, B9.5, B9-A0	5, 2, 11
2M J11081509-7733531	Glass I, T33A, P23, Bel12	Flat	5.7 ± 0.1	3.4 ± 0.2	1.9 ± 0.4	1.2 ± 0.4	0.5 ± 0.4	G3-G7, G3-K3	13,1
2M J11083896-7743513	IRN, P24, Bel2	I	161. ± 0.9	96.9 ± 1.1	40.9 ± 0.7	18.5 ± 0.5	6.9 ± 0.3	<M0	1
2M J11083905-7716042	T35, ISO151, C15	II	0.4 ± 0.1	0.2 ± 0.1	...	...	...	M0, K8	17, 1
2M J11085464-7702129	VY Cha, T38, Sz29	II	0.2 ± 0.1	...	...	...	...	M0.5, M0.5	3,1
2M J11091812-7630292	CHXR79, Hn9, P29	II	0.1 ± 0.1	...	...	...	...	M0.75-M1.75	1
2M J11092855-7633281	ISO192, CaINa2	I	8.5 ± 0.3	5.8 ± 1.0	2.4 ± 0.9	1.1 ± 0.7	0.9 ± 0.5	M6.5	4
2M J11092266-7634320	C1-6, P30	II	1.2 ± 0.3	0.5 ± 0.9	...	...	...	M0.75-M1.75	1
2M J11092379-7623207	VZ Cha, T40	II	0.4 ± 0.1	0.4 ± 0.1	0.3 ± 0.1	0.3 ± 0.1	0.3 ± 0.1	K6, K6	3, 7
2M J11094192-7634584	C1-25, ISO199, Cam1-79	II	0.2 ± 0.3	1.8 ± 0.1	...	0.1 ± 0.7	1.0 ± 0.5	<M0	7
2M J11094621-7634463	Hn10e, P34	II	...	5.2 ± 1.2	3.0 ± 0.9	1.9 ± 0.7	1.0 ± 0.5	M3.25	1
2M J11094742-7726290	B43, P35, ISO207, Bel18	II	0.1 ± 0.1	0.2 ± 0.1	0.3 ± 0.1	0.3 ± 0.1	0.2 ± 0.2	M3.25, M1	1, 14
2M J11095340-7634255	FM Cha, P37, HM23, Bel62	II	11.4 ± 0.3	7.1 ± 1.0	2.8 ± 0.9	1.7 ± 0.7	0.6 ± 0.5	K4-K6	1
2M J11095407-7629253	Sz33, T43, P38	II	0.3 ± 0.1	0.3 ± 0.4	...	...	...	M0, M2, M2	8, 9, 1
2M J11095505-7632409	C1-2, P39, ISO226	Flat	1.8 ± 0.3	1.7 ± 1.1	...	...	...	<M0	3
2M J11095873-7737088	WX Cha, T45, P40	II	0.2 ± 0.1	0.2 ± 0.1	...	...	...	K7-M0, K7-M0, M1.25	2, 3, 7
2M J11100010-7634578	WW Cha, P41, T44	II	22.2 ± 0.3	20.9 ± 1.0	15.1 ± 0.9	8.5 ± 0.7	4.8 ± 0.5	K5, <K6	1, 2, 3
2M J11100369-7633291	Hn11, P42, ISO232	II	...	0.9 ± 0.9	...	...	...	K8	1
2M J11100704-7629376	WY Cha, T46, Ced112-IRS6	II	0.2 ± 0.1	0.1 ± 0.1	...	...	...	K7, M0, M0	2, 3, 7
2M J11101141-7635292	ISO237, C27, Bel31	II	1.7 ± 0.4	2.1 ± 1.1	1.2 ± 0.9	...	...	M1.5, M0, K5.5	4, 9, 1
2M J11103801-7732399	CHXR47, P45	II	0.1 ± 0.1	...	...	...	...	K3, K3	11, 18
2M J11104959-7717517	HM27, T47, P46	II	0.5 ± 0.1	0.4 ± 0.1	...	...	...	K7, M2	3,1
2M J11111083-7641574	ESO Ha 569	II	0.2 ± 0.1	0.2 ± 0.2	...	...	...	K7, M2.5	5, 3
2M J11113965-7620152	XX Cha, T49, Sz39	II	0.2 ± 0.1	...	0.1 ± 0.1	0.1 ± 0.1	...	M0, M2, M1. 5-2.5	2, 3, 1
2M J11114632-7620092	CHX 18N, Cam1-103	II	0.3 ± 0.1	0.2 ± 0.1	0.2 ± 0.1	0.1 ± 0.1	...	K1, K3, K6	15, 18, 1
2M J11122772-7644223	CV Cha, T52	II	2.1 ± 0.1	1.1 ± 0.1	0.6 ± 0.1	0.3 ± 0.2	0.2 ± 0.1	G8, G9, G8, K0	5, 6, 2, 3
2M J11124268-7722230	T54, B51	II/TD	0.3 ± 0.1	...	...	...	...	K0, G5-K0, G5	2, 13, 15

Notes. For a full list of identifiers for each source, please refer to Table 1 of Luhman et al. (2008). Identifiers: *IRN, LkHα.., HM.., ..Cha, Glass..*: Gavin & Strom (1992); *Ced..*: Prusti et al. (1991); *CHXR..*: Lawson et al. (1996); *B..*: Alcala (1994); Baud et al. (1984); *HH..*: Schwartz (1991); *P..*: Persi et al. (2000); *C..*: Cambresy et al. (1998); *Bel..*: Belloche et al. (2011).

References. 1) Luhman (2004); 2) Rydgen (1980); 3) Appenzeller et al. (1983); 4) Gomez & Mardones (2003); 5) Henize & Mendoza (1973); 6) Appenzeller (1977); 7) Luhman (2007); 8) Gomez & Persi (2002); 9) Saffe et al. (2003); 10) Luhman & Muench (2008); 11) Whittet et al. (1987); 12) Comeron et al. (1999); 13) Feigelson & Kriss (1989); 14) Comeron et al. (2004); 15) Walter (1992); 16) Bradner & Zinnecker (1997); 17) Gavin & Strom (1992); 18) Covino et al. (1997a); 19) Joergens & Guenther (2001).

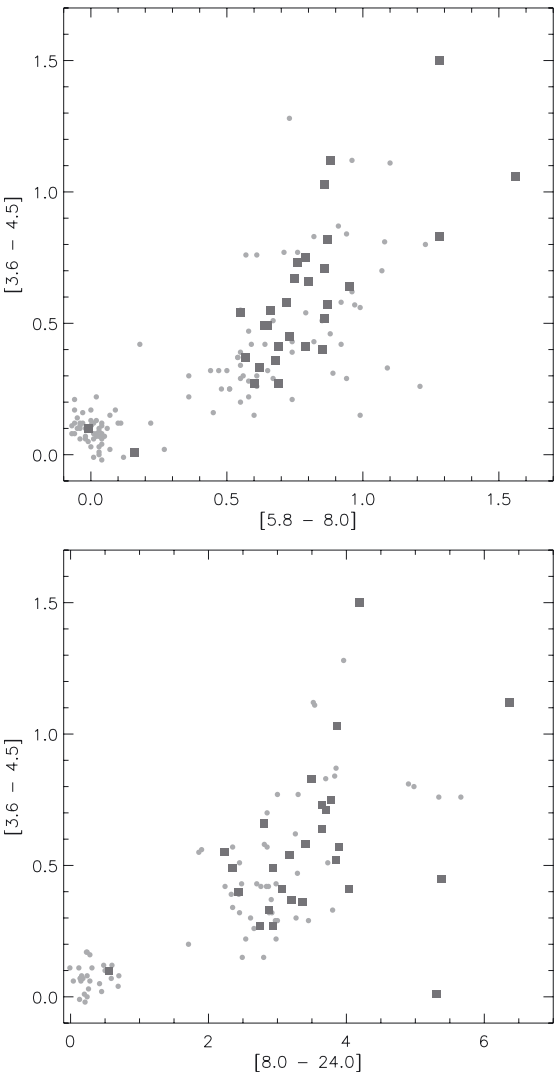

Fig. 2. *Above*: *Spitzer* IRAC [3.6–4.5] vs. [5.8–8.0] colour–colour figure derived from the Luhman et al. (2008) photometry. *Below*: *Spitzer* IRAC-MIPS [3.6–4.5] vs. [8.0–24] colour–colour figure of the Luhman et al. (2008) YSOs. Grey dots indicate the Luhman et al. (2008) identified YSOs. The black symbols indicate those YSOs detected with *Herschel*. The group of YSOs clustered around [0,0] in both diagrams are the class III sources.

types, listed in Table 1, these are mostly M and K type stars. Specifically, all of the *Herschel* detected YSOs in the northern Ced 112 cluster surrounding HD 97300 have spectral type mid to late M. The southern population is more distributed but the majority are still M-K stars. Therefore, it is more likely that these stars represent the youngest segment of the Cha I population and still retain thick outer disks and/or envelopes.

4.3. Herschel fluxes and colours of detected sources

Figure 5 shows the *Herschel* $\log(F_{160})$ vs. $\log(F_{160}/F_{250})$ flux-ratio diagram, where the black circles indicate the known class I objects, the asterisks identify the flat spectrum objects, the grey triangles mark the known class II sources, the inverted triangles indicate the transition disc members, and the open squares mark the positions of those *Herschel* sources also identified by Belloche et al. (2011) at 870 μm. While the difference in 160 μm flux between the three groups is not highly significant, the class II sources extend to fainter fluxes than the protostars

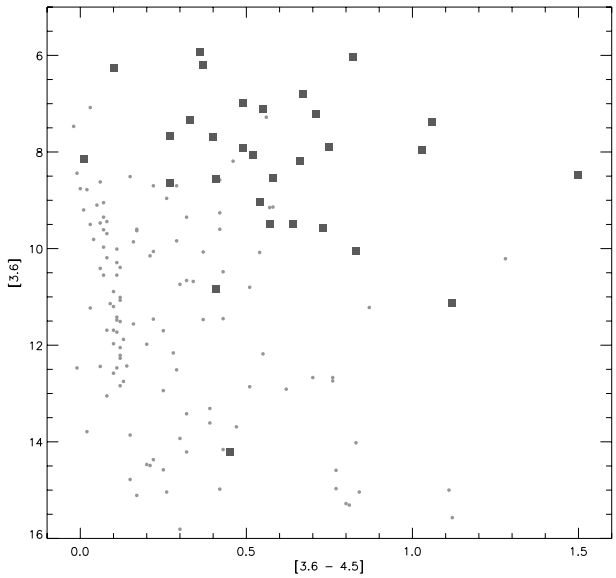

Fig. 3. *Spitzer* IRAC [3.6] vs. [3.6–4.5] colour–magnitude figure derived from the Luhman et al. (2008) photometry, with grey dots indicating the Luhman et al. (2008) identified YSOs and black squares indicating those YSOs detected with *Herschel*. Only those YSOs with $m_{3.6\ \mu m}$ brighter than 10 are likely to be detected with *Herschel*. The *Herschel* detected sample is complete for sources with [3.6–4.5] colour >0.6 and $m_{3.6} < 10$.

or candidate cores. There is a distinct colour difference between the known YSOs and the Belloche identified *Herschel* objects. The YSOs have a bluer colour at $\log(F_{160}/F_{250})$ than the cores, where the median colour of the class II sample was found to be $0.19^{+0.05}_{-0.12}$ and the median colour of the candidate cores was found to be $-0.29^{+0.22}_{-0.26}$. Though the difference in median colour is only significant to 1-σ, it is indicative of a trend towards bluer $\log(F_{160}/F_{250})$ ratios for the more evolved young stars. The median fluxes for the protostars (class I and flat spectrum), class II, and candidate core detections at each of the five *Herschel* wavelengths are presented in Table 2. Table 3 lists the median colours for each class of object for the three colours shown in Figs. 5–7. In both tables the uncertainties presented give the interquartile range: [upper quartile – median] and [median – lower quartile], where the lower quartile is the value below which 25% of the sample fall, the upper quartile is the value below which 75% of the sample lie, and the interquartile range is the range of values which encompasses the central 50% of the sample.

Figures 6 and 7 show two *Herschel* colour–colour ratio diagrams: $\log(F_{160}/F_{250})$ vs. $\log(F_{250}/F_{350})$ and $\log(F_{160}/F_{250})$ vs. $\log(F_{350}/F_{500})$ where the symbols are the same as in Fig. 5. Again, the trend in median colour in $\log(F_{160}/F_{250})$ can be clearly seen. There are no trends in the median colours between the known YSOs and the candidate cores at either the $\log(F_{250}/F_{350})$ or $\log(F_{350}/F_{500})$ colours. The range in colours is similar for the young stars and the candidate prestellar cores, though the candidate cores do extend towards redder $\log(F_{350}/F_{500})$ colours, which is expected of more deeply embedded and younger objects, which are expected to be colder and to emit at longer wavelengths than the more evolved young stars.

Another comparison that can be made is that between the colours and fluxes of the identified protostellar class I/flat spectrum objects and the more evolved class II young stars. Our investigation indicates that there is some difference in the fluxes

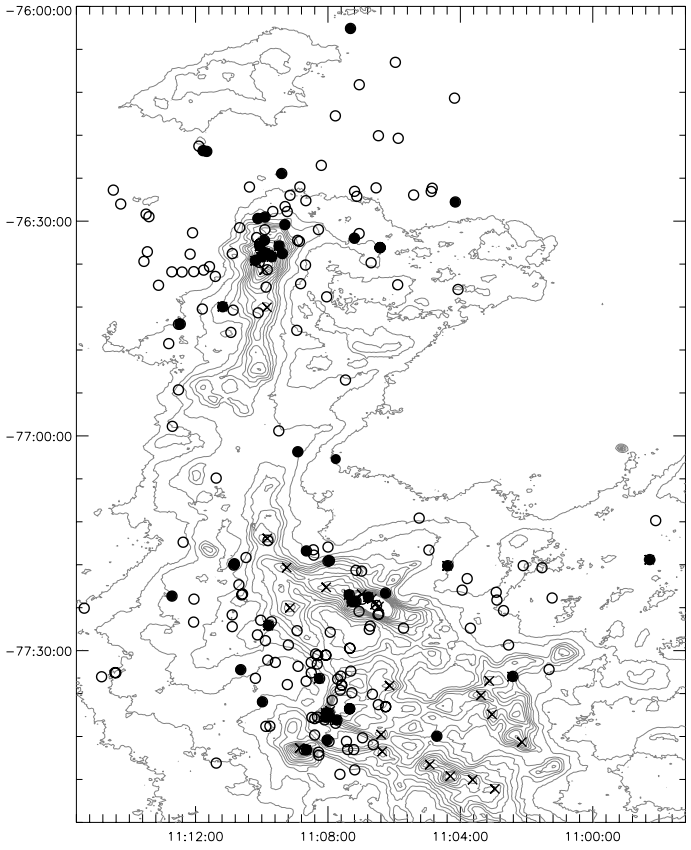

Fig. 4. Contours of the SPIRE 500 μm mosaic, showing the elongated structure of the dust, shown at levels of 30, 40, 45, 50, 55, 60, 65% of the peak flux 13.4 Jy/beam. The open circles indicate the positions of the *Spitzer* identified YSOs (Luhman et al. 2008), the filled circles are those YSOs also detected with *Herschel*. The "*x*" symbols mark the positions of the *Herschel* sources matched to Belloche et al. (2011) detections; excluding three which are off-field to the west. It may be noted that the *Herschel* detected YSOs are mainly located in and near the centres of the three clusters. North is up and east is to the left, coordinates are given in Equ J2000.

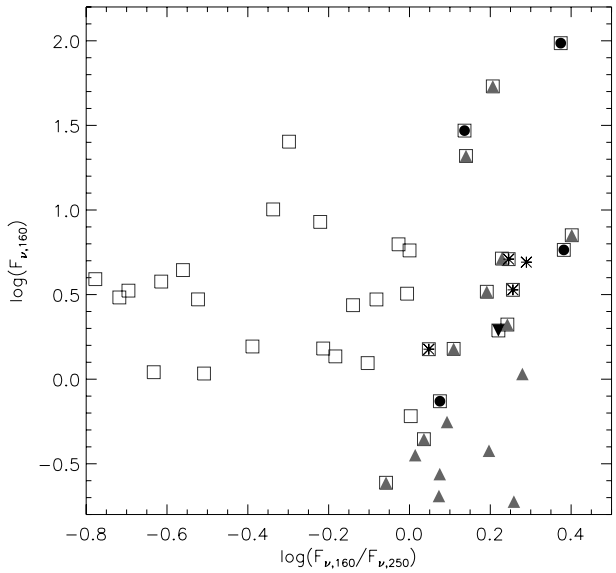

Fig. 5. Flux-colour ratio figure $\log(F_{160})$ vs. $\log(F_{160}/F_{250})$ showing the *Herschel* photometry of all sources with required photometry detected in the field. The grey triangles represent the Luhman et al. (2008) class II objects, the class I objects are shown by black circles. The flat spectrum objects are marked by asterisks. The inverted triangles mark the transition disc objects. The *Herschel* detections with a counterpart in the Belloche et al. (2011) catalogue are marked with open squares. These objects may be class 0 sources or starless/prestellar cores. No trend in magnitude is present, however the known YSOs exhibit a bluer colour than the candidate cores. Note that redward is to the left in this diagram.

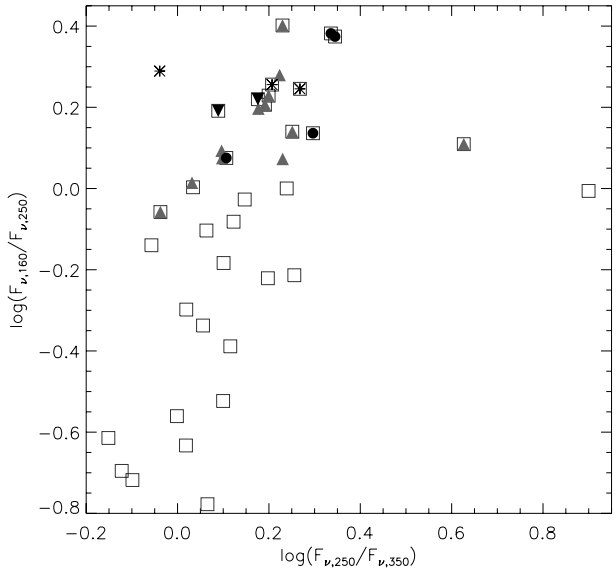

Fig. 6. Colour–colour figure $\log(F_{160}/F_{250})$ vs. $\log(F_{250}/F_{350})$ showing the *Herschel* photometry of all sources with required photometry detected in the field. The symbols are the same as in Fig. 5. The known YSOs appear bluer at $\log(F_{160}/F_{250})$ than the candidate cores. However there is no difference in colour at $\log(F_{250}/F_{350})$. Note that redward is towards the left in this diagram.

but not the colours between the protostellar and class II members of the cluster detected by *Herschel*. The protostars have brighter median fluxes at the four shorter wavelengths than the class II objects. Neither group have a significant peak in their median fluxes across the five *Herschel* bands: the median fluxes of the class II sources appear to be flat across the five wavelengths, while the protostars show some indication of a decrease in flux with increasing wavelength. There is no significant difference in colour between the protostellar and class II sources, though the class II show consistently redder median colours than the protostars.

One *Herschel* detection is of particular interest: the variable star CS Cha, which exhibits IRAC colours similar to that of a field star, indicating that it has an optically thin inner disk, while exhibiting a large colour excess at [8–24], indicating that it is a transitional disc object. Kim et al. (2009) support its classification as a transition disc in their *Spitzer* IRS survey. Its *Herschel* colours and fluxes are similar to those of the other detected YSOs, its $\log(F_{160}/F_{250})$ colour of 0.22 gives it a blue colour similar to those of the class II objects. Identified as a binary system by Guenther et al. (2007), Nagel et al. (2012) model CS Cha as possessing both a circumbinary and circumstellar disks, complicating the classification of CS Cha as a straightforward transition disk. We also detect two other class II sources which Kim et al. (2009) and Manoj et al. (2011) reclassify as likely transition disks. These two sources, SZ Cha and T54, do not exhibit obvious transition disc colours on the *Spitzer* ccds, being more similar to class II. SZ Cha exhibits a similarly blue *Herschel* colour as CS Cha, with $\log(F_{160}/F_{250})$ colour of 0.19. T54 is only reliably detected at 70 μm.

Table 2. Median fluxes [Jy] of the *Herschel* detected sources in Cha I as a function of object type.

Classification	$\log(F_{\nu,70})$	$\log(F_{\nu,160})$	$\log(F_{\nu,250})$	$\log(F_{\nu,350})$	$\log(F_{\nu,500})$
Protostars (11)	$0.75^{+0.18}_{-0.99}$ (10)	$0.69^{+0.07}_{-0.51}$ (10)	$0.40^{+0.93}_{-0.13}$ (08)	$0.19^{+0.84}_{-0.15}$ (08)	$-0.28^{+1.04}_{-0.22}$ (09)
Class II (33)	$-0.40^{+0.63}_{-0.36}$ (31)	$-0.28^{+0.54}_{-0.33}$ (27)	$-0.35^{+0.79}_{-0.27}$ (17)	$-0.49^{+0.73}_{-0.30}$ (15)	$-0.02^{+0.04}_{-0.59}$ (10)
Cand. cores (30)	$0.37^{+0.08}_{-1.07}$ (04)	$0.48^{+0.16}_{-0.35}$ (24)	$0.76^{+0.44}_{-0.22}$ (21)	$0.68^{+0.54}_{-0.34}$ (27)	$0.68^{+0.37}_{-0.49}$ (30)

Notes. Numbers in brackets indicate the number of sources considered.

Table 3. Median colour of the *Herschel* detected sources in Cha I as a function of object type.

Classification	$\log(F_{160}/F_{250})$	$\log(F_{250}/F_{350})$	$\log(F_{350}/F_{500})$
Protostars (11)	$0.26^{+0.12}_{-0.12}$ (08)	$0.29^{+0.05}_{-0.09}$ (08)	$0.28^{+0.15}_{-0.17}$ (08)
Class II (33)	$0.19^{+0.05}_{-0.12}$ (16)	$0.19^{+0.04}_{-0.09}$ (16)	$0.26^{+0.04}_{-0.16}$ (10)
Cand. cores (30)	$-0.29^{+0.22}_{-0.26}$ (21)	$0.06^{+0.08}_{-0.06}$ (21)	$0.21^{+0.07}_{-0.23}$ (27)

Notes. Numbers in brackets indicate the number of sources considered.

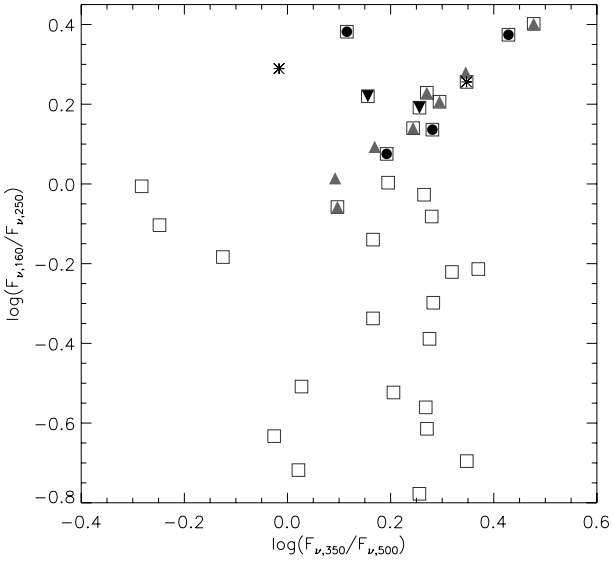

Fig. 7. Colour–colour figure $\log(F_{160}/F_{250})$ vs. $\log(F_{350}/F_{500})$ showing the *Herschel* photometry of all sources detected in the field. The symbols are the same as in Fig. 5. The known YSOs appear bluer at $\log(F_{160}/F_{250})$ than the candidate cores. There is, however, no difference in colour at $\log(F_{350}/F_{500})$. Note that redward is towards the left in this diagram.

5. Conclusions

The Chamaeleon I star forming cloud has been observed as part of the *Herschel* Gould Belt survey of the entire Chamaeleon complex, utilising PACS and SPIRE parallel mode observations at 70, 160, 250, 350, and 500 μm to map the cloud with complete coverage at all five wavelengths. The main results from our initial study of Cha I are:

- Using the recently developed *getsources* source extraction software we have detected 397 reliable sources in the observed Cha I field, 77 of which are previously known YSOs or cores. Of these 77, forty-nine are identified as YSOs. The other 28 detections are candidate class 0 members, or starless or prestellar cores associated with Belloche et al. (2011) detections. In addition to these, we also detect two outflow features, two emission features from the ring near HD 97300, and five CO clumps (Haikala et al. 2005). The remaining 311 detections may be associated with the cluster; however the majority lie in regions of low A_V, and are likely to be background galaxies.
- Of the 49 identified young stars, one is considered a class 0 protostar, four are class I protostars, six are flat spectrum protostars, thirty-four are class II pre-main sequence stars, three are considered to be transition disc objects: CS Cha, SZ Cha, and T54. Only one of the known class III young stars is detected in the *Herschel* images, Ced 110 IRS2.
- By comparing the *Spitzer* colours and magnitudes of the detected and non-detected young members of the cloud we find no difference in colour between those young stars detected by *Herschel* and those that are not, with no obvious trend towards redder IRAC colours discernible. Those objects with the brightest 3.6 μm magnitudes are the most likely to be detected with 80% detected with $m_{3.6} < 8.5$, 43% are detected with *Herschel* for $m_{3.6} < 10.5$, and 4% are detected for $m_{3.6} > 10.5$.
- The *Herschel* fluxes indicate that the protostellar and candidate cores have brighter fluxes at most wavelengths when compared to the class II sources. The candidate cores are more reddened than the known protostars and PMS members. There is no significant difference in colour between the protostellar and class II sources for any colour from *Herschel* wavelengths.
- The three detected transition disc sources in the cluster exhibit bluer $\log(F_{160}/F_{250})$ colours than the median value of the class II sources.

The *Herschel* observations provide unprecedented resolution in the far-IR, especially at 70 μm, enabling us to both extend the study of the known YSOs into the cold dust regime, and to observe embedded class 0 protostars and prestellar cores. Further work in the region is underway to understand the filamentary structure of the cloud and to model the SEDs of the *Herschel* sources to gain a greater understanding of the environment in which stars form and their evolution from embedded protostar to evolved stellar system.

Acknowledgements. We would like to thank the anonymous referee for their very helpful comments on the paper. P.R. and N.L.J.C. acknowledge support from the Belgian Federal Science Policy Office via the PRODEX Programme of ESA. The *Herschel* spacecraft was designed, built, tested, and launched under a contract to ESA managed by the *Herschel/Planck* project team by an

industrial consortium under the overall responsibility of the prime contractor Thales Alenia Space (Cannes), and including Astrium (Friedrichshafen) responsible for the payload module and for system testing at spacecraft level, Thales Alenia Space (Turin) responsible for the service module, and Astrium (Toulouse) responsible for the telescope, with in excess of a hundred subcontractors. PACS has been developed by a consortium of institutes led by MPE (Germany) and including UVIE (Austria); KUL, CSL, IMEC (Belgium); CEA, OAMP (France); MPIA (Germany); IFSI, OAP/AOT, OAA/CAISMI, LENS, SISSA (Italy); IAC (Spain). This development has been supported by the funding agencies BMVIT (Austria), ESA-PRODEX (Belgium), CEA/CNES (France), DLR (Germany), ASI (Italy), and CICT/MCT (Spain). SPIRE has been developed by a consortium of institutes led by Cardiff Univ. (UK) and including Univ. Lethbridge (Canada); NAOC (China); CEA, LAM (France); IFSI, Univ. Padua (Italy); IAC (Spain); Stockholm Observatory (Sweden); Imperial College London, RAL, UCL-MSSL, UKATC, Univ. Sussex (UK); and Caltech, JPL, NHSC, Univ. Colorado (USA). This development has been supported by national funding agencies: CSA (Canada); NAOC (China); CEA, CNES, CNRS (France); ASI (Italy); MCINN (Spain); SNSB (Sweden); STFC (UK); and NASA (USA). This publication makes use of data products from the Two Micron All Sky Survey, which is a joint project of the University of Massachusetts and the Infrared Processing and Analysis Center/California Institute of Technology, funded by the National Aeronautics and Space Administration and the National Science Foundation. This research has made use of the NASA/IPAC Infrared Science Archive, which is operated by the Jet Propulsion Laboratory, California Institute of Technology, under contract with the National Aeronautics and Space Administration. This research has made use of the SIMBAD database, operated at CDS, Strasbourg, France. This research has made use of Aladin.

References

Alcala, J. M. 1994, Ph.D. Thesis, Ruprecht-Karls-Universitat, Heidelberg
Appenzeller, I. 1977, A&A, 61, 21
Appenzeller, I., Jankovics, I., & Krautter, J. 1983, A&AS, 53, 291
André, Ph., Men'shchikov, A., Bontemps, S., et al. 2010, A&A, 518, L102
Arzoumanian, D., André, Ph., Didelon, P., et al. 2011, A&A, 529, A6
Baud, B., Beintema, D. A., Wesselius, P. R., et al. 1984, ApJ, 278, 53
Belloche, A., Schuller, F., Parise, B., et al. 2011, A&A, 527, A145
Bradner, W., & Zinnecker, H. 1997, A&A, 321, 220
Cambresy, L., Copet, E., Epchtein, N., et al. 1998, A&A, 338, 977
Cederblad, S. 1946, Meddelanden frn Lunds Astronomiska Observatorium, Ser. II, 119, 1
Clements, D. L., Rigby, E., Maddox, S., et al. 2010, A&A, 518, L8
Comeron, F., Rieke, G. H., & Neuhauser, R. 1999, A&A, 343, 477
Comeron, F., Reipurth, B., Henry, A., & Fernandez, M. 2004, A&A, 417, 583
Covino, E., Alcala, J. M., Allain, S., et al. 1997a, A&A, 328, 187
Feigelson, E. D., & Kriss, G. A. 1989, ApJ, 338, 262
Feigelson, E. D., & Lawson, W. A. 2004, A&A, ApJ, 614, 267
Gavin, S. 1992, ApJ, 385, 217
Gomez, M., & Kenyon, S. J. 2001, AJ, 121, 974
Gomez, M., & Mardones, D. 2003, AJ, 125, 2134
Gomez, M., & Persi, P. 2002, A&A, 389, 494
Griffin, M. J., Abergel, A., Abreu, A., et al. 2010, A&A, 518, L3
Guedel, M. 2009, SIMBOL-X: Focusing on the Hard X-ray Universe, AIP Conf. Proc., 1126, 341
Guenther, E. W., Esposito, M., Mundt, R., et al. 2007, A&A, 367, 1147
Haikala, l. K., Harju, J., Mattila, K., & Toriseva, M. 2005, A&A, 431, 149
Henize, K. G., & Mendoza, E. E. 1973, ApJ, 180, 115
Joergens, V., & Guenther, E. 2001, A&A, 379, L9
Kim, K. H., Watson, D. M., Manoj, P., et al. 2009, ApJ, 700, 1017
Kóspál, A., Prusti, T., Merin, B., et al. 2012, A&A, 541, A71
Lawson, et al. 1996, MNRAS, 271, 967
Luhman, K. L. 2004, ApJ, 602, 816
Luhman, K. L. 2007, ApJS, 173, 104
Luhman, K. L. 2008, Chamaeleon in Handbook of Star Forming Regions, Vol. II, ASP, ed. B. Reipurth
Luhman, K. L., & Muench, A. A. 2008, ApJ, 684, 654
Luhman, K. L., Allen, L. E., Allen, P. R., et al. 2008, ApJ, 675, 1375
Manoj, P., Kim, K. H., Furlan, E., et al. 2011, ApJSS, 193, 11
Men'shchikov, A., Andr'e, Ph., Didelon, P., et al. 2010, A&A, 518, L103
Men'shchikov, A., Andr'e, Ph., Didelon, P., et al. 2012, A&A, 542, A81
Nagel, E., Espaillat, C., D'Alessio, P., & Calvet, N. 2012, ApJ, 747, 139
Ott, S. 2010, Astronomical Data Analysis Software and Systems XIX, eds. Y. Mizumoto, K.-I. Morita, & M. Ohishi, ASP Conf. Ser., 434, 139
Persi, P., Marenzi, A. R., Olofsson, G., et al. 2000, A&A, 357, 219
Pilbratt, G. L., Riedinger, J. R., Passvogel, T., et al. 2010, A&A, 518, L1
Poglitsch, A., Waelkens, C., Geis, N., et al. 2010, A&A, 518, L2
Prusti, T., Clark, F. O., Whittet, D. C. B., et al. 1991, MNRAS, 251, 303
Reipurth, B., Nyman, L.-A., & Chini, R. 1996, A&A, 314, 258
Roussel, H. 2012 [arXiv:1205.2576]
Rydgen, A. E. 1980, AJ, 85, 444
Saffe, C., Randich, S., Mardones, D., et al. 2003, A&A, 409, 993
Schwartz, R. D. 1991, Scient. Rep. 11, ed. B. Reipurth (ESO), 93
Schwartz, R. D., & Henize, K. G. 1983, AJ, 88, L665
Stelzer, B., Micela, G., & Nuehauser, R. 2004, A&A, 423, 1029
Walter, F. M. 1992, AJ, 104, 758
Whittet, D. C. B., Kirrane, T. M., Kilkenny, D., et al. 1987, MNRAS, 224, 497
Whittet, D. C. B., Prusti, T., Franco, G. A. P., et al. 1997, A&A, 327, 1194
Winston, E., Megeath, S. T., Wolk, S. J., et al. 2007, ApJ, 669, 493